

Dimensional crossover in dipolar magnetic layers

This article has been downloaded from IOPscience. Please scroll down to see the full text article.

2000 J. Phys. A: Math. Gen. 33 1

(<http://iopscience.iop.org/0305-4470/33/1/301>)

View [the table of contents for this issue](#), or go to the [journal homepage](#) for more

Download details:

IP Address: 171.66.16.118

The article was downloaded on 02/06/2010 at 08:01

Please note that [terms and conditions apply](#).

Dimensional crossover in dipolar magnetic layers

M Bulenda[†], U C Täuber[‡] and F Schwabl^{†§}

[†] Institut für Theoretische Physik, Physik Department der Technischen Universität München, James-Frank Straße, D-85747 Garching, Germany

[‡] Physics Department, Virginia Polytechnic Institute and State University, Blacksburg, VA 24061-0435, USA

Received 21 June 1999

Abstract. We investigate the static critical behaviour of a uniaxial magnetic layer, with finite thickness L in one direction, yet infinitely extended in the remaining d dimensions. The magnetic dipole-dipole interaction is taken into account. We apply a variant of Wilson's momentum shell renormalization group approach to describe the crossover between the critical behaviour of the 3D Ising, 2D Ising, 3D uniaxial dipolar, and the 2D uniaxial dipolar universality classes. The corresponding renormalization group fixed points are in addition to different effective dimensionalities characterized by distinct analytic structures of the propagator, and are consequently associated with varying upper critical dimensions. While the limiting cases can be discussed by means of dimensional ϵ expansions with respect to the appropriate upper critical dimensions, respectively, the crossover features must be addressed in terms of the renormalization group flow trajectories at fixed dimensionality d .

1. Introduction

Layered magnetic systems are of obvious technological importance, e.g. in magnetic storage devices. Presently, magneto-optic storage devices based on amorphous GdTbFe and TbFeCo alloys are in commercial use, allowing for storage densities of up to 10^8 bits cm^{-2} . In the future, however, Pt/Co, Pd/Co and Co/Au multilayers of a few ångström thickness are expected to lead to four times as high storage capacities. On the purely theoretical side, they furthermore represent an intriguing model system with the competing exchange- and dipolar-dominated universality classes on the one hand, and the dimensional crossover between three and two effective dimensions on the other. The mathematical description of the associated crossover features within the framework of the renormalization group theory is technically challenging, as it involves both varying analytic structures of the propagators, and different upper critical dimensions for the associated renormalization group fixed points. The aim of this paper is to demonstrate that such a unifying crossover description is feasible, even with the aforementioned difficulties at hand. For a layered uniaxial magnetic system of finite width L in one direction and with dipolar interactions taken into account, the renormalization program is explicitly performed to one-loop order for the entire crossover regime by means of a variant of Wilson's momentum shell method at fixed transverse dimension d . Moreover, it is shown that the scheme described here encompasses all the relevant universality classes involved, and the critical exponents at each renormalization group fixed point may be computed within an ϵ expansion about the respective upper critical dimensions.

§ Author to whom correspondence should be addressed.

In the theory of phase transitions there has been long-standing interest in the critical properties of finite systems as well as in the influence of the magnetic dipole–dipole interaction on static and dynamic critical behaviour. The first investigations for the crossover behaviour between the different critical regimes in dipolar systems date back 30 years: in their pioneering work, Larkin and Khmel’nitskiĭ [1] showed that the upper critical dimension of a uniaxial magnet with magnetic dipole–dipole interaction is reduced by one as compared with the pure Ising system. The mathematical description of the crossover in a 3D system with easy axis and dipolar forces therefore necessitated a renormalization scheme capable of dealing with varying upper critical dimensions associated with the different non-trivial fixed points. Modifying the generalized dimensional regularization method by Amit and Goldschmidt [2], such a description was developed in [3] for the crossover between the Ising and 3D uniaxial dipolar fixed points of a uniaxial dipolar magnet, and in [4] for the crossover from isotropic to directed percolation. This approach was then applied to an even more complex scenario by Ried *et al* [5], who considered the crossovers between all four possible fixed points of a uniaxial dipolar system, taking the finiteness of the anisotropy into account. It should be noted, though, that all these calculations employed the harmonic dipolar propagator originally derived in [6]. Yet this propagator is adequate only in the case of a 3D infinite system, or, more generally, for any system of the same dimensionality as the one used for computing the effective magnetic dipole–dipole interaction. It is therefore *not* applicable for 3D electrodynamics, if the system itself is 2D, for example, or is finite in one or more directions.

Static critical behaviour in finite systems with purely short-range interactions was investigated in [7–10]. Here, the asymptotic critical behaviour was addressed, and no crossover scaling functions were calculated. Dimensional crossovers were studied in the context of quantum phase transitions by Chakravarty *et al* for quantum antiferromagnets [11], and by O’Connor and Stephens for an Ising system between four and three dimensions [12]. Yet we are not aware of any work concerning the critical behaviour in a finite system that takes into account the magnetic dipole–dipole interaction.

In this paper we go beyond the cited literature in describing the crossover scenario for a uniaxial magnetic system with dipolar interactions that is infinitely extended in d dimensions, but has a finite thickness L in one additional direction. For simplicity, we assume that the anisotropy energy is larger than all other relevant energy scales, and hence only take into account the Ising-type up–down symmetry. In the case of $d = 2$, such a system is supposed to exhibit four different regimes of non-trivial critical behaviour, in addition to the classical one described by mean-field critical exponents; these are described by the 3D Ising, 2D Ising, 3D uniaxial dipolar, and 2D uniaxial dipolar universality classes, respectively. As will be shown, these regimes are characterized in addition to varying effective system dimensions by different analytic forms of the propagator, which originate in the dipole–dipole interaction. Consequently, three different upper critical dimensions d_c emerge: for the Ising systems, $D_c = 4$ and $d_c = 4$, respectively, for the 3D uniaxial dipolar system $D_c = 3$, and finally the upper critical dimension for the truly asymptotic critical behaviour of a 2D uniaxial dipolar system with an easy axis in the system’s plane will be demonstrated to be $d_c = \frac{7}{2}$.

This paper is organized as follows: in section 2 we introduce the effective Hamiltonian (free energy functional) and specifically the propagator (two-point correlation function in Gaussian approximation) that is to be used for our calculations. In section 3 we explain our variant of the momentum shell renormalization method devised to mathematically describe the crossover scenarios. In section 4 the resulting renormalization group flow equations are derived to one-loop order and discussed. Section 5 contains the resulting limiting cases within the ϵ expansions in the vicinities of the appropriate upper critical dimensions. In section 6 the crossovers between the critical fixed points are discussed in terms of the renormalization

group trajectories. We conclude with a summary and brief discussion in section 7.

2. Effective Hamiltonian

At first we need to deduce an effective free energy functional that is capable of capturing the crossover features we are aiming at. However, at this point we encounter the difficulty that the analytic forms of the propagators (Gaussian two-point correlation functions) describing uniaxial dipolar magnetic systems are quite different depending on the dimensionality $D = d + 1$ of the system. We employ periodic boundary conditions to avoid surface effects, in which we are not specifically interested here. Rather we are concerned with the effect of the system's limited extent in one space direction as such.

Denoting the part of the wavevector \mathbf{k} in the direction of the easy axis of the magnetization as \mathbf{q} , and the perpendicular component as \mathbf{p} , $\mathbf{k} = \mathbf{q} + \mathbf{p}$, the propagators appear as follows: in the case of a 3D system, the relevant part of the inverse propagator is of the form $G_0(\mathbf{q}, \mathbf{p})^{-1} = r + ck^2 + gq^2/p^2$ [13], while for a 2D system containing the easy axis, $G_0(\mathbf{q}, \mathbf{p})^{-1} = r + ck^2 + gq^2/k$, with $k = |\mathbf{k}|$ [14]. On the other hand, if the easy axis is aligned perpendicular to the 2D plane, the result is of the form $G_0(\mathbf{q}, \mathbf{p})^{-1} = r + ck^2 - gk$ [14]. Here $r = T - T_c^0$ denotes the temperature distance to the mean-field transition temperature T_c^0 , c is a constant describing the stiffness of the system with respect to inhomogeneous order parameter configurations, and g measures the strength of the dipole–dipole interaction as compared with the exchange interaction.

As our task is the description of a system with finite thickness, we have to apply some care in the derivation of the appropriate form of the propagator. The contribution to the free energy stemming from the dipole–dipole interaction between the magnetic moments connected to the spin variables $S_{\mathbf{R}}$ at lattice sites \mathbf{R} reads

$$W_D = g \sum_{\mathbf{R}_1 \neq \mathbf{R}_2} \sum_{\alpha\beta} A^{\alpha\beta}(\mathbf{R}_1, \mathbf{R}_2) S_{\mathbf{R}_1}^\alpha S_{\mathbf{R}_2}^\beta \quad (1)$$

with the dipole tensor in real space being defined as

$$A^{\alpha\beta}(\mathbf{R}_1, \mathbf{R}_2) = \frac{\delta^{\alpha\beta}}{|\mathbf{R}_1 - \mathbf{R}_2|^3} - \frac{3(\mathbf{R}_1 - \mathbf{R}_2)^\alpha (\mathbf{R}_1 - \mathbf{R}_2)^\beta}{|\mathbf{R}_1 - \mathbf{R}_2|^5}. \quad (2)$$

Here, the indices α and β denote real space vector components. In Fourier space, the dipole sum for a cubic lattice becomes

$$A^{\alpha\beta}(\mathbf{k}) = A_{2d}^{\alpha\beta}(\mathbf{p}) + \frac{2\pi}{a_0} \sum_{\rho \neq 0} e^{iq\rho} \sum_g \frac{(\mathbf{p} - \mathbf{g})^\alpha (\mathbf{p} - \mathbf{g})^\beta}{|\mathbf{p} - \mathbf{g}|} e^{-|\rho||\mathbf{p} - \mathbf{g}|} \quad (3)$$

if the spins are oriented in the plane, and

$$A^{\alpha\beta}(\mathbf{k}) = A_{2d}^{\alpha\beta}(\mathbf{p}) - \frac{2\pi}{a_0} \sum_{\rho \neq 0} e^{iq\rho} \sum_g |\mathbf{p} - \mathbf{g}| e^{-|\rho||\mathbf{p} - \mathbf{g}|} \quad (4)$$

if the spins are oriented perpendicular to the plane [14]. $A_{2d}^{\alpha\beta}(\mathbf{p})$ represents the dipole tensor for the 2D system, with wavevectors \mathbf{p} and associated 2D reciprocal lattice vectors \mathbf{g} . ρ is the discrete coordinate of a lattice plane along the finite direction, and a_0 and q indicate the corresponding lattice constant and wavenumbers, respectively. For the later treatment by means of the renormalization group technique, we need only retain the relevant long-wavelength contributions, and may thus simplify the above expressions by restricting the reciprocal wavevector sums to $\mathbf{g} = 0$ only. This part yields the correct limits for the propagators of both the 3D and the 2D system.

Finally, we expand the resulting expressions to obtain the long-wavelength limits. For the easy axis lying in the plane we find the following form:

$$A^{\alpha\beta}(\mathbf{q}, \mathbf{p}) = (1 + f_1) \frac{p^\alpha p^\beta}{p} + f_2 \frac{p^\alpha p^\beta}{p} q^2 + f_3 p^\alpha p^\beta + f_4 p^\alpha p^\beta p + f_5 p^\alpha p^\beta q^2 + \mathcal{O}(p^3 q^2, p^4, p^2 q^4). \quad (5)$$

Denoting by $2N + 1$ the number of lattice planes in the finite direction, $L = 2N a_0$, the N -dependent functions f_i read:

$$f_1 = 2N \quad (6)$$

$$f_2 = -\frac{a_0^2}{6} N(1 + 3N + 2N^2) \quad (7)$$

$$f_3 = -a_0 N(1 + N) \quad (8)$$

$$f_4 = \frac{a_0^2}{6} N(1 + 3N + 2N^2) \quad (9)$$

$$f_5 = \frac{a_0^3}{4} N^2(1 + N)^2. \quad (10)$$

If the easy axis is aligned perpendicular to the plane, we arrive at

$$A^{\alpha\beta}(\mathbf{q}, \mathbf{p}) = -(1 + \tilde{f}_1)p - \tilde{f}_3 p^2 - \tilde{f}_2 q^2 p + \mathcal{O}(p^3 q^2, p^4) \quad (11)$$

instead, with the N -dependent functions

$$\tilde{f}_1 = 2N \quad (12)$$

$$\tilde{f}_2 = -\frac{a_0^2}{6} N(1 + 3N + 2N^2) \quad (13)$$

$$\tilde{f}_3 = -a_0 N(1 + N). \quad (14)$$

We note that the long-wavelength expansion does *not* commute with taking the limit of infinite system thickness, $N \rightarrow \infty$. Consequently, the above formulae are strictly valid only for finite system thickness L . Nonetheless we shall see that the method to be described below will yield the correct results even for the 3D system.

We are now in the position to write down the effective Hamiltonians that serve as starting points for our renormalization group treatment. Dealing with a finite system in one direction, we symbolically write the sum over all Fourier modes as

$$\int_{\mathbf{k}} \dots \equiv \frac{1}{(2\pi)^d} \int_{0 < |\mathbf{p}| < \Lambda} d^d p \frac{1}{L} \sum_{q = \frac{2\pi}{L} n} \dots, n \in Z. \quad (15)$$

In the limit of the fully infinite system, $L \rightarrow \infty$, this definition is to be replaced with

$$\int_{\mathbf{k}} \dots \equiv \frac{1}{(2\pi)^D} \int_{0 < |\mathbf{p}| < \Lambda} d^d p \int d\mathbf{q} \quad \text{where } D = d + 1 \quad (16)$$

denotes the dimension of the entire system. In both situations, Λ represents a cutoff whose numerical value is not relevant for the critical behaviour. Therefore we shall use $\Lambda = 1$ throughout the paper (in appropriate dimensionless units). Notice that we only apply the cutoff for the wavevector components in the plane, and *not* for the perpendicular component.

Thus the final effective free energy for a *layer with easy axis in the plane* assumes the form

$$\mathcal{H}_{2d,\parallel} = \frac{1}{2} \int_{\mathbf{k}} \left[r_0 + c_0 k^2 + g(1 + f_1) \frac{p_i^2}{p} + g f_2 \frac{p_i^2}{p} q^2 \right]$$

$$\begin{aligned}
& +gf_3p_l^2 + gf_4p_l^2p + gf_5p_l^2q^2 \Big] S_0(\mathbf{k})S_0(-\mathbf{k}) \\
& + \frac{u_0}{4!} \int_{k_1} \int_{k_2} \int_{k_3} \int_{k_4} S_0(\mathbf{k}_1)S_0(\mathbf{k}_2)S_0(\mathbf{k}_3)S_0(\mathbf{k}_4)\delta\left(\sum_{i=1}^4 \mathbf{k}_i\right)
\end{aligned} \tag{17}$$

where q again is the wavevector component perpendicular to the system, and \mathbf{p} the in-plane part, with p_l denoting the component pointing along the direction of the easy axis. The Hamiltonian for a layer with the easy axis perpendicular to the plane reads

$$\begin{aligned}
\mathcal{H}_{2d,\perp} = & \frac{1}{2} \int_{\mathbf{k}} [r_0 + c_0k^2 - g(1 + \tilde{f}_1)p - g\tilde{f}_3p^2 - g\tilde{f}_2q^2p] S_0(\mathbf{k})S_0(-\mathbf{k}) \\
& + \frac{u_0}{4!} \int_{k_1} \int_{k_2} \int_{k_3} \int_{k_4} S_0(\mathbf{k}_1)S_0(\mathbf{k}_2)S_0(\mathbf{k}_3)S_0(\mathbf{k}_4)\delta\left(\sum_{i=1}^4 \mathbf{k}_i\right).
\end{aligned} \tag{18}$$

For a 3D system we find instead [13]

$$\begin{aligned}
\mathcal{H}_{3d} = & \frac{1}{2} \int_{\mathbf{k}} \left[r_0 + c_0k^2 + g\frac{q^2}{p^2} \right] S_0(\mathbf{k})S_0(-\mathbf{k}) \\
& + \frac{u_0}{4!} \int_{k_1} \int_{k_2} \int_{k_3} \int_{k_4} S_0(\mathbf{k}_1)S_0(\mathbf{k}_2)S_0(\mathbf{k}_3)S_0(\mathbf{k}_4)\delta\left(\sum_{i=1}^4 \mathbf{k}_i\right)
\end{aligned} \tag{19}$$

where q denotes the component of \mathbf{k} along the direction of the easy axis, and \mathbf{p} is the part of \mathbf{k} perpendicular to the easy axis.

Thus, henceforth we are concerned with the description of critical phenomena with those three different Hamiltonians. The free energy of the 3D system cannot be recovered any more from the layered Hamiltonian (18) by taking the limit of infinite layer thickness $N \rightarrow \infty$. Nevertheless we will show that all the limiting cases, including the 3D uniaxial dipolar one, are described correctly within our scheme.

3. Renormalization scheme

As already mentioned, the expected critical regimes are clearly characterized by different system dimensions, as well as different analytical structures of the propagators, leading to different upper critical dimensions. Hence we need a renormalization scheme capable of dealing with these different fixed points in a unified manner, and sufficiently flexible as to describe the crossovers between them. In addition, we aim to capture the crossover features with the correct transition temperature $T_c(L, g)$ (see appendix A) of the finite system, and not with that of the infinite system as in [7–10], where furthermore the studied systems were infinite in at most one direction (and consequently do not display a proper phase transition). As our system asymptotically becomes 2D, we have to circumvent problems with infrared divergences appearing in field-theoretic approaches, e.g. dimensional regularization, for such low-dimensional systems [2, 3, 12, 15]. One more aspect is that we must include the full gradient terms in order to describe the crossover between Ising and uniaxial dipolar behaviour, and cannot restrict ourselves to merely the most relevant parts in one of the limits as in [16].

In order to accommodate all these requirements, we apply a variant of Wilson's momentum shell renormalization method, similar to the one used previously by Chakravarty *et al* for the crossover theory of a quantum nonlinear sigma model [11]. (Certainly, to one-loop order, the ensuing wavevector shell integrals over \mathbf{p} , followed by the summations over q , are technically considerably easier to perform in this approach as compared with the field theory version.) One renormalization transformation now consists of two steps: starting

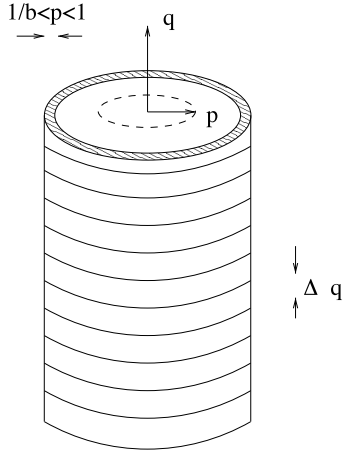


Figure 1. The modes being integrated out during one renormalization step.

from the effective Hamiltonian functional \mathcal{H} , we first integrate out the short-wavelength order parameter fluctuations in the partition function $Z(\mathcal{H})$ in the d directions of the plane, and then sum over the wavevector components perpendicular to the plane (without any cutoff). In wavevector space, the modes to be integrated out are depicted in figure 1. In the second step, the wavevectors \mathbf{k} , spin variables $S_{\mathbf{k}}$, and system thickness L are rescaled with an as yet arbitrary scale factor $b > 1$, and a spin rescaling factor $\zeta(b)$ which eventually has to be chosen appropriately in terms of b :

$$\mathbf{k}' = b\mathbf{k} \quad (20)$$

$$S'_{\mathbf{k}'} = \zeta(b)^{-1} S_{\mathbf{k}} \quad (21)$$

$$L' = b^{-1}L. \quad (22)$$

After this transformation, we arrive at a new free energy functional \mathcal{H}' of the same form as before, but with renormalized coefficients fulfilling $Z(\mathcal{H}) = Z(\mathcal{H}')$. By successively evaluating partial partition functions, and subsequently applying scale transformations, we approach the interesting infrared behaviour of our theory, and in effect map the perturbationally inaccessible critical regime onto a region in parameter space where perturbation theory may be applied. As usual the critical regions themselves, characterized by algebraic singularities and scale-invariance, are represented by fixed points of the renormalization (semi-)group transformation.

We apply this scheme in the framework of the one-loop approximation, however, refraining from any ϵ expansion, for in our problem there is no unique and common upper critical dimension. We choose our rescaling factors to be isotropic in contrast to, e.g. [16]; this induces apparently diverging parameters under the renormalization flow [13]. Yet these may be readily absorbed into appropriately defined *effective couplings*, by means of which we can describe the associated crossover features [2–5]. In contrast to [17] we define the spin rescaling factor $\zeta(b)$ such that the gradient term of the Hamiltonian functional remains unchanged during the renormalization procedure. Again, this helps us capture the entire crossover regime, while the advantages of the scheme in [17], where the term with the lowest wavevector power is held fixed, are gathered through the construction and discussion of suitable effective couplings.

4. Renormalization group flow equations

In this section, we compute the differential renormalization group flow equations for a magnetic layer with the easy axis in the plane, a layer with easy axis perpendicular to the plane, and a 3D system. Our starting points will be the different Hamiltonians (17), (18) and (19), respectively, for these systems. Following through the renormalization scheme as described in the previous section, with $b^\ell = e^{\delta\ell}$, $\delta \rightarrow 0$, for the finite systems we arrive at the following differential flow equations for the system thickness L , the coefficient c of the gradient term, and the strength g of the dipole–dipole interaction:

$$\frac{dL}{d\ell} = -L \quad (23)$$

$$\frac{dc}{d\ell} = 0 \quad (24)$$

$$\frac{dg}{d\ell} = g. \quad (25)$$

Before moving on to the flow equations specific to the different systems, we discuss these differential equations common to both finite systems. The flow equation (23) for the layer thickness L is *exact*, and is solved by $L = L_0 e^{-\ell}$ with $\ell \rightarrow +\infty$ in the infrared limit. Thus, the fixed points for the layer thickness are $L = \infty$ and $L = 0$, with $L = 0$ being infrared-stable. Hence the asymptotic critical behaviour is that of the 2D system: as the correlation length diverges, the system thickness becomes irrelevant in the renormalization group sense (as indicated by the negative sign on the rhs in equation (23)). The coefficient c of the gradient term in the free energy functional is held fixed during the renormalization procedure through the choice of the spin rescaling factor ζ , whence equation (23) follows from the definition. The strength of the non-analytic dipole–dipole interaction g cannot be renormalized perturbationally, and consequently equation (24) simply follows from dimensional analysis and holds to all orders in perturbation theory. Its solution reads $g = g_0 e^\ell$, and the fixed points for the dipole strength are $g = 0$ and $g = \infty$, and the latter is infrared-stable. As to be expected, the critical behaviour of the system is eventually dominated by the dipole interaction. This is a consequence of the long-range character of the dipolar forces in contrast to the short-ranged exchange interactions. For the derivation of the remaining flow equations we have to distinguish between the different systems under consideration.

First we focus on the layer with the easy axis in the plane. The remaining differential flow equations read

$$\frac{df_1}{d\ell} = 0 \quad (26)$$

$$\frac{df_2}{d\ell} = -2f_2 \quad (27)$$

$$\frac{df_3}{d\ell} = -f_3 \quad (28)$$

$$\frac{df_4}{d\ell} = -2f_4 \quad (29)$$

$$\frac{df_5}{d\ell} = -3f_5 \quad (30)$$

following, to one-loop order, simply from dimensional analysis, and

$$\frac{dr}{d\ell} = 2r + \frac{u}{2} \frac{1}{(2\pi)^d} \frac{\Lambda^2}{L} \int_0^{2\pi} d\theta \frac{L/2}{\sqrt{a(\theta)b(\theta)}} \coth \left(\frac{L}{2} \sqrt{\frac{a(\theta)}{b(\theta)}} \right) \quad (31)$$

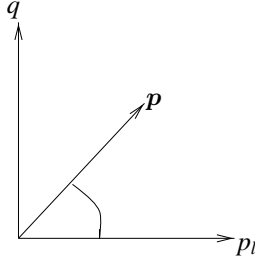


Figure 2. Definitions of p_l and the angle θ .

$$\frac{du}{d\ell} = (3-d)u - \frac{3}{2}u^2 \frac{1}{(2\pi)^d} \frac{\Lambda^2}{L} \int_0^{2\pi} d\theta \frac{L/4}{b(\theta)^{1/2} a(\theta)^{3/2}} \frac{1}{\sinh\left(\frac{L}{2} \sqrt{\frac{a(\theta)}{b(\theta)}}\right)} \times \left[\cosh\left(\frac{L}{2} \sqrt{\frac{a(\theta)}{b(\theta)}}\right) + \frac{L}{2} \sqrt{\frac{a(\theta)}{b(\theta)}} \frac{1}{\sinh\left(\frac{L}{2} \sqrt{\frac{a(\theta)}{b(\theta)}}\right)} \right] \quad (32)$$

to one-loop order. Here θ indicates the angle between the wavevector component in the plane \mathbf{p} and the direction of the easy axis p_l (see figure 2). The θ -dependent functions a and b are defined as follows:

$$a(\theta) = r + c\Lambda^2 + g(1+f_1)\Lambda \cos^2 \theta + gf_3\Lambda^2 \cos^2 \theta + gf_4\Lambda^3 \cos^2 \theta \quad (33)$$

$$b(\theta) = c + gf_2\Lambda \cos^2 \theta + gf_5\Lambda^2 \cos^2 \theta. \quad (34)$$

While the coefficient f_1 remains invariant under the renormalization group flow, the irrelevant parameters f_2, f_3, f_4 trivially flow towards their stable fixed points $f_2 = f_3 = f_4 = 0$. Notice that there exist no fixed points with $f_i = \infty$, because the functions f_i were only defined for a finite system thickness. The more intricate flow equations for the temperature variable r and the non-linear coupling u will be discussed in the following sections.

For a layer with easy axis perpendicular to the plane, on the other hand, we find the following flow equations:

$$\frac{d\tilde{f}_1}{d\ell} = 0 \quad (35)$$

$$\frac{d\tilde{f}_2}{d\ell} = -2\tilde{f}_2 \quad (36)$$

$$\frac{d\tilde{f}_3}{d\ell} = -\tilde{f}_3 \quad (37)$$

from power counting, and

$$\frac{dr}{d\ell} = 2r + \frac{u}{2} \frac{K}{L} \sum_q \frac{1}{a + bq^2} \quad (38)$$

$$\frac{du}{d\ell} = (3-d)u - \frac{3}{2}u^2 \frac{K}{L} \sum_q \frac{1}{(a + bq^2)^2}. \quad (39)$$

Here the functions a and b are defined as follows:

$$a = r + (c - g\tilde{f}_3)\Lambda^2 - g(1 + \tilde{f}_1)\Lambda \quad (40)$$

$$b = c - g\tilde{f}_2\Lambda - g\tilde{f}_4\Lambda^2 \quad (41)$$

and we have introduced and used the dimension-dependent factor

$$K = \frac{\Lambda^d}{(2\pi)^{d-1}}. \quad (42)$$

Closer inspection reveals that in the case of an easy axis perpendicular to the layer and with infinite anisotropy, the propagator is not positive definite. Inevitably, therefore, the terms in the sums in equations (38) and (39) will become negative under the renormalization group flow. This indicates an instability at the non-zero wavevector, and the ground state of the system becomes inhomogeneous, with the characteristic wavelength of the emerging spatial structures given by that instability wavevector (the typical size of the structures appearing in the low-temperature phase is estimated in appendix B). At any rate, it is impossible to analyse the asymptotic critical behaviour with the effective Hamiltonian (18) which was obtained via an expansion about a presumed homogeneous ground state. Hence, in the remainder of this paper we shall concentrate on the study of the critical behaviour of a layer with in-plane easy axis, and on the 3D limit.

For a 3D system, finally we obtain the renormalization group flow equations

$$\frac{dc}{d\ell} = 0 \quad (43)$$

$$\frac{dg}{d\ell} = 2g \quad (44)$$

$$\frac{dr}{d\ell} = 2r + \frac{u}{4} \frac{K}{\sqrt{(c + \frac{g}{\Lambda^2})(r + c\Lambda^2)}} \quad (45)$$

$$\frac{du}{d\ell} = (4 - D)u - \frac{3}{8}u^2 \frac{K}{\sqrt{(c + \frac{g}{\Lambda^2})(r + c\Lambda^2)^3}}. \quad (46)$$

These equations do not appear as the limit $L \rightarrow \infty$ of the flow equations of the layer (31) and (32), where the effective free energy has already been adjusted to the specific geometries. In order to arrive at the correct 3D expression, one has to start from the correct, full Hamiltonian (19), as the long-wavelength limit and the limit $N \rightarrow \infty$ do not commute, as already mentioned in section 2. Again, c is held fixed by construction, and the renormalization group flow for the relevant dipole–dipole interaction has the unstable fixed point $g = 0$ and the infrared-stable fixed point $g = \infty$.

Before discussing the different critical regions and the crossover between them within our scheme, we focus on the obvious limiting cases of the general flow equations, and compute the critical exponents within dimensional ϵ expansions about the appropriate upper critical dimensions, respectively.

5. Limiting cases in ϵ expansions

5.1. 3D Ising limit

We arrive at the limit of the flow equations at the *unstable* fixed point $g = 0$ and $L = \infty$ by expanding the hyperbolic functions in the differential flow equations (31) and (32) for the layer in the limit of large argument. Assuringly, we can alternatively take the flow equations for the 3D system (44) and (45) with $g = 0$. With either approach, we obtain

$$\frac{dr}{d\ell} = 2r + \frac{u}{4} \frac{K}{\sqrt{c(r + c\Lambda^2)}} \quad (47)$$

$$\frac{du}{d\ell} = \epsilon u - \frac{3}{8} u^2 \frac{K}{\sqrt{c(r + c\Lambda^2)^3}} \quad (48)$$

where $\epsilon = 4 - D$ gives the distance to the upper critical dimension $D_c = 4$ of the system. From these equations we get the critical exponents at the non-trivial fixed point to first order in ϵ ,

$$r^* = -\frac{\epsilon}{3} c\Lambda^2 + \mathcal{O}(\epsilon^2) \quad (49)$$

$$Ku^* = \frac{8}{3} \epsilon \frac{1}{\sqrt{c(c\Lambda^2)^3}} + \mathcal{O}(\epsilon^2) \quad (50)$$

as usual via the eigenvalues of the linearized flow equations. The results, consistently expanded to first order in $\epsilon = 4 - D$, are

$$\nu = \frac{1}{2} \left(1 + \frac{\epsilon}{6} + \mathcal{O}(\epsilon^2) \right) \quad (51)$$

$$\eta = 0 + \mathcal{O}(\epsilon^2) \quad (52)$$

$$\gamma = 1 + \frac{\epsilon}{6} + \mathcal{O}(\epsilon^2) \quad (53)$$

in accordance with the well known results for the single-component ϕ^4 model (see, e.g., [15]), with $\epsilon = 1$ in $D = d + 1 = 3$ dimensions.

5.2. 3D uniaxial dipolar limit

Next, we discuss the second limiting case in three dimensions, namely the uniaxial dipolar fixed point at $g = \infty$ and $L = \infty$. We have to start from equations (44) and (45). Upon introducing the effective expansion parameter [3]

$$v_{\text{eff}} = u/\sqrt{g} \quad (54)$$

we arrive at the flow equations

$$\frac{dr}{d\ell} = 2r + \frac{v_{\text{eff}}}{4} \frac{K\Lambda}{\sqrt{r + c\Lambda^2}} \quad (55)$$

$$\frac{dv_{\text{eff}}}{d\ell} = \epsilon v_{\text{eff}} - \frac{3}{8} v_{\text{eff}}^2 \frac{K\Lambda}{(r + c\Lambda^2)^{3/2}} \quad (56)$$

where now $\epsilon = 3 - D$ was used for the deviation from the upper critical dimension $D_c = 3$. In $D = d + 1 = 3$ dimensions, we thus expect the mean-field critical exponents with logarithmic corrections. This is in agreement with previous work addressing the critical behaviour of a 3D uniaxial dipolar magnet [1, 3, 8].

5.3. Two-dimensional Ising limit

In the limit of absent dipole–dipole interaction $g = 0$ and zero thickness $L = 0$ we have to expand the hyperbolic functions in the flow equations (31) and (32) for vanishing arguments. With the effective coupling

$$v_{\text{eff}} = u/L \quad (57)$$

this procedure gives the flow equations

$$\frac{dr}{d\ell} = 2r + \frac{v_{\text{eff}}}{2} \frac{K}{(r + c\Lambda^2)} \quad (58)$$

$$\frac{dv_{\text{eff}}}{d\ell} = \epsilon v_{\text{eff}} - \frac{3}{2} v_{\text{eff}}^2 \frac{K}{(r + c\Lambda^2)^2} \quad (59)$$

here, however, $\epsilon = 4 - d$ ($= 2$ in $D = d + 1 = 3$ dimensions). Linearizing in the vicinity of the non-trivial fixed point

$$r^* = -\frac{\epsilon}{6}c\Lambda^2 + \mathcal{O}(\epsilon^2) \quad (60)$$

$$K v_{\text{eff}}^* = \frac{2}{3}\epsilon c^2 \Lambda^4 + \mathcal{O}(\epsilon^2) \quad (61)$$

we find the critical exponents to order $\epsilon = 4 - d$ ($= 2$ in two dimensions):

$$\nu = \frac{1}{2} \left(1 + \frac{\epsilon}{6} + \mathcal{O}(\epsilon^2) \right) \quad (62)$$

$$\eta = 0 + \mathcal{O}(\epsilon^2) \quad (63)$$

$$\gamma = 1 + \frac{\epsilon}{6} + \mathcal{O}(\epsilon^2). \quad (64)$$

Thus, this low-dimensional limit is also correctly included in the general flow equations. Note that in terms of the expansion parameter ϵ , these exponents of course coincide with the 3D Ising case above. Remember, however, that there $\epsilon = 4 - D = 1$ and here $\epsilon = 4 - d = 2$ in the relevant physical situation $D = d + 1 = 3$.

5.4. 2D uniaxial dipolar limit, in-plane easy axis

This limit is especially interesting for two reasons: first, it represents the asymptotic critical behaviour of the system under consideration; and second it is intriguing in its own right because we are aware of only one other reference which addresses the critical behaviour of a 2D uniaxial dipolar system with the easy axis in the plane [18]. Yet, in [18] the critical exponents are not presented explicitly. Using the same approximation for the hyperbolic functions as before and introducing the effective expansion parameter

$$v_{\text{eff}} = \frac{u}{L\sqrt{g}} \quad (65)$$

we obtain the asymptotic flow equations

$$\frac{dr}{d\ell} = 2r + \frac{v_{\text{eff}}}{2^d \pi^{d-1}} \frac{\Lambda^2}{\sqrt{(r + c\Lambda^2)(1 + f_1)\Lambda}} \quad (66)$$

$$\frac{dv_{\text{eff}}}{d\ell} = \left(\frac{7}{2} - d \right) v_{\text{eff}} - \frac{3}{2} \frac{v_{\text{eff}}^2}{2^d \pi^{d-1}} \frac{\Lambda^2}{\sqrt{(r + c\Lambda^2)^3(1 + f_1)\Lambda}}. \quad (67)$$

Consequently, we identify the upper critical dimension here as $d_c = \frac{7}{2}$. The non-trivial fixed point to order $\epsilon = \frac{7}{2} - d$ is

$$r^* = -\frac{\epsilon}{3}c\Lambda^2 + \mathcal{O}(\epsilon^2) \quad (68)$$

$$v_{\text{eff}}^* = \frac{2}{3}\epsilon \frac{2^d \pi^{d-1}}{\Lambda^2} [(1 + f_1)\Lambda]^{1/2} (c\Lambda^2)^{3/2} + \mathcal{O}(\epsilon^2). \quad (69)$$

Linearization near this fixed point leads to the following asymptotic critical exponents to first order in $\epsilon = \frac{7}{2} - d$:

$$\nu = \frac{1}{2} \left(1 + \frac{\epsilon}{6} + \mathcal{O}(\epsilon^2) \right) \quad (70)$$

$$\eta = 0 + \mathcal{O}(\epsilon^2) \quad (71)$$

$$\gamma = 1 + \frac{\epsilon}{6} + \mathcal{O}(\epsilon^2). \quad (72)$$

Once again, these exponents look superficially identical to those of the short-range Ising model; yet the critical dimension and the value of ϵ is different: in $d = 2$, $\epsilon = \frac{1}{2}$. In summary, all the asymptotic limits are correctly included in the general flow equations.

6. Crossover analysis

In the previous section, we have demonstrated the consistency of our general approach with the ϵ expansions near the respective critical dimensions of the limiting universality classes. We now proceed to the application of our scheme to the description of the actual crossovers between the different critical regions.

6.1. General procedure

First we want to describe the general procedure to be used. We use the calculated renormalization group flow equations to investigate the scale dependence of the effective interaction parameters. Specifically, we map the critical region onto a region in parameter space that is perturbationally accessible. In the infrared region, we can, e.g., evaluate the static susceptibility perturbationally, and thus obtain the static susceptibility χ in the critical region via the solution of the renormalization group equation that takes the form (the Fisher exponent η vanishes in the one-loop approximation)

$$\chi(r_0, g_0, u_0, L_0, \mathbf{k}) = e^{2\ell} \chi(r(\ell), g(\ell), u(\ell), L(\ell), \mathbf{k}(\ell)). \quad (73)$$

Therefrom we can infer the *effective* exponent

$$\gamma_{\text{eff}}(\tau) = \frac{d \ln \chi^{-1}}{d \ln \tau} \quad (74)$$

as function of reduced temperature $\tau = \frac{T-T_c}{T_c}$. This method was used first in [19] in the framework of an ϵ expansion; but here we make no use of any dimensional expansion, but perform all our calculations numerically at a *fixed* dimension. The one-loop recursion relations are then solved without recourse to any additional approximation.

It is vital here to introduce an appropriate effective expansion parameter that yields the correct 3D and 2D limits as given in the previous section. This effective coupling has to have a finite limit at the asymptotic fixed point below the upper critical dimension of the system. As suggested by the flow equations in section 4, we use the effective couplings

$$v_{\text{eff}} = u \int_0^{2\pi} d\theta \frac{1}{\sqrt{a(\theta)b(\theta)}} \coth \left(\frac{L}{2} \sqrt{\frac{a(\theta)}{b(\theta)}} \right) \quad (75)$$

for the layer with in-plane easy axis, and

$$v_{\text{eff}} = \frac{2\pi}{\sqrt{r + c\Lambda^2}} \frac{u}{\sqrt{g}} \quad (76)$$

for the 3D case. Then within our methodical framework, the critical regions are again represented by fixed points of the renormalization group transformation, and we may obtain the critical exponents from the eigenvalues of the linearized transformation in the vicinity of the fixed points (yet without applying any further approximation-like dimensional expansions).

6.2. Limiting cases at fixed dimension

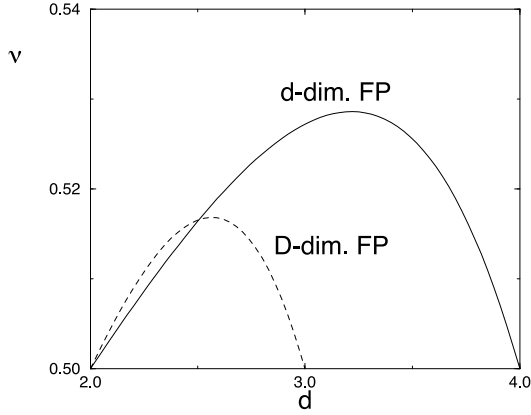
The appearance of renormalization group fixed points to first order in an expansion does not necessarily guarantee the existence of fixed points if we refrain from an ϵ expansion. At first, therefore, we have to re-calculate the non-trivial fixed points and the associated critical exponents at fixed dimensionality $D = d + 1$. The actual fixed points thus obtained are listed in table 1. The eigenvalues of the linearized flow equations can be easily calculated analytically, and are not presented explicitly here. In table 2 we give the numerical values

Table 1. Renormalization group fixed points at fixed dimension to one-loop order.

Fixed point	r^*	v_{eff}^*
3D Ising	$-\frac{2}{3}(4-D)c\Lambda^d[2+\frac{2}{3}(4-D)]^{-1}$	$\frac{16\pi}{3K_d}(4-D)\sqrt{(r^*+c\Lambda^2)}$
2D Ising	$-(4-d)c\Lambda^2/(4-d+6)$	$\frac{16\pi}{K_d}(4-d)c\Lambda^2/(4-d+6)$
3D uniaxial dipolar	0	0
2D uniaxial dipolar	$-(\frac{7}{2}-d)c\Lambda^2/(\frac{7}{2}-d+3)$	$\frac{16\pi}{K_d}(\frac{7}{2}-d)c\Lambda^2/(\frac{7}{2}-d+3)$

Table 2. Numerically determined fixed-point values and critical exponents.

Fixed point	r^*	v_{eff}^*	L^*	γ	ν
3D Ising	-0.25	78.95	∞	1	$\frac{1}{2}$
2D Ising	-0.25	78.95	0	1	$\frac{1}{2}$
3D uniaxial dipolar	0	0	∞	1	$\frac{1}{2}$
2D uniaxial dipolar	-0.33	105.27	0	0.94	0.47

**Figure 3.** Ising fixed-point values of the critical exponent ν as function of dimension.

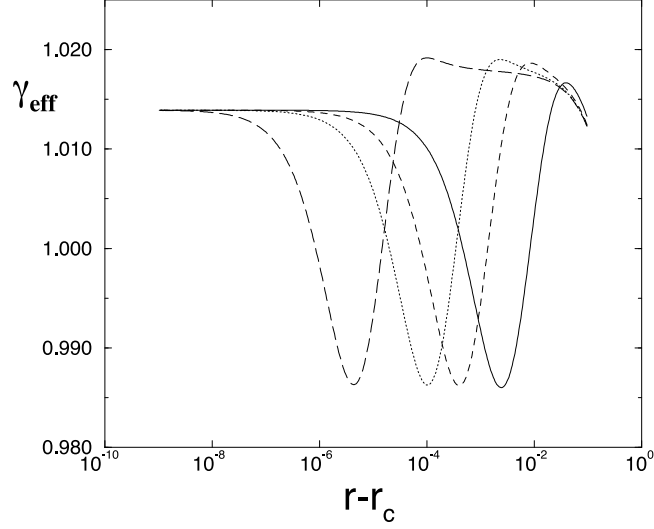
of the fixed points as well as the critical exponents ν and γ for the system with two infinite dimensions ($D = d+1 = 3$). As is readily seen, the numerical results for the critical exponents cannot be judged as good approximations to their realistic values. The reason is very likely the inadequacy of the one-loop approximation. An unfortunate artefact of the system under consideration is that the actual fixed-point values as well as the critical exponents for the 3D Ising and the 2D Ising limit turn out to be identical to this order. This happens to be the case *only* in this dimension $D = 3$, as can be seen from figure 3, where we plot the numerical values of the critical exponent ν at both the higher and lower dimensional fixed points, respectively, versus the dimension. This artificial coincidence only appears at the dimensions $d = \frac{5}{2}$ and $d = 2$, the physical dimension in which we are interested. Nevertheless, we shall argue for the usefulness of our scheme in describing different crossover features.

6.3. Dimensional crossover

The first crossover that we want to analyse within our scheme is the dimensional crossover for an Ising layer (dipolar strength $g = 0$). In order to circumvent the unfortunate exponent coincidence mentioned above, we evaluate the crossover features between 3.2 and 2.2 dimensions. In this situation, we are not only able to calculate the flow equations describing the

Table 3. Numerical fixed-point values for an Ising layer with $d = 2.2$.

Fixed point	r^*	v_{eff}^*	L^*	ν
3.2D Ising	-0.2105	96.0267	∞	0.5090
2.2D Ising	-0.2308	105.2601	0	0.5070

**Figure 4.** Layer with vanishing dipole–dipole interaction. Effective critical exponent γ_{eff} versus reduced temperature $\tau \sim r - r_c$ for systems of different thicknesses: $N = 20$ (full line), $N = 50$ (dashed), $N = 100$ (dotted), $N = 500$ (long-dashed).

crossover, but also the effective critical exponent γ_{eff} as a function of the reduced temperature τ . The corresponding renormalization group fixed-point values are listed in table 3. The effective exponent γ_{eff} describing the crossover is calculated numerically for different layer thicknesses L , and the results are plotted in figure 4. It can be seen that at a temperature sufficiently far from the transition temperature, the susceptibility exponent takes on the value of the higher-dimensional fixed point, then with decreasing temperature goes through a minimum which is obviously independent of the layer thickness, and finally reaches the asymptotic value of the lower-dimensional fixed point. The thicker the layer, the longer the system remains in the higher-dimensional critical region as the temperature is lowered, and the later it reaches the asymptotic critical region. This is fully to be expected based on straightforward considerations.

6.4. Crossover exchange-dominated/dipole-dominated

Next we apply our scheme to the fully 3D system, where the crossover occurs between the region with dominating exchange interactions and the asymptotic region with dominating dipole–dipole interaction. Because the numerical values of the critical exponents happen to be identical at both these fixed points within our scheme at fixed dimension $D = 3$, see table 2, the crossover cannot be noticed at all in the temperature dependence of the effective critical exponent γ_{eff} . However, we can discuss the crossover by means of the flow diagrams in the $r-v_{\text{eff}}$ plane. In figure 5, the flow diagram is depicted for different initial temperatures (which cannot be distinguished in this graph, however). The arrow indicates the starting point of the trajectories. These first approach the unstable Ising fixed point (filled circle on the right), before

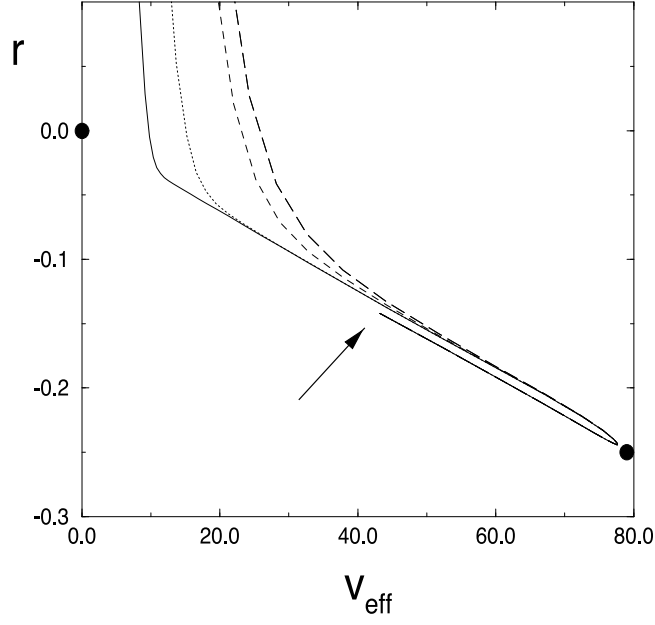


Figure 5. Infinite 3D dipolar system. Flow of the effective coupling v_{eff} and temperature variable r for different initial temperature values, with $g_0 = 10^{-5}$ and $u_0 = 5$: $r \approx r_c$ (full line), $r - r_c = 6.42 \times 10^{-11}$ (dotted), $r - r_c = 6.66 \times 10^{-9}$ (dashed), $r - r_c = 1.67 \times 10^{-8}$ (long-dashed).

finally approaching the asymptotically stable fixed point that represents the uniaxial dipolar regime (filled circle on the left). Eventually the trajectories diverge in the temperature variable r due to the numerically inevitably finite distance from the critical point (even small inaccuracies in determining the true critical temperature will eventually blow up under renormalization). In figure 6 we depict the same scenario for a stronger dipole–dipole interaction. In this situation, the unstable fixed point is not approached as closely as before, and the stable fixed point is approached more closely before the trajectories eventually diverge to $r \rightarrow \infty$ due to the finite distance from the critical temperature.

6.5. Crossover features of the dipolar layer

At last, we address the description of the crossover scenario for a dipolar magnetic layer with in-plane easy axis. As the starting point is the Hamiltonian (17), which is only defined for finite system thickness, we cannot reach the fixed point corresponding to the 3D uniaxial dipolar region. The crossover will thus occur between the critical regions of the 3D and 2D Ising systems, and the 2D uniaxial dipolar regime, which represents the asymptotic universality class. As the numerical fixed-point values of the effective coupling, the temperature variable, and the effective critical exponent of the static susceptibility γ_{eff} of the 2D and the 3D Ising fixed point are identical, we illustrate the flow trajectories in 3D parameter space, consisting of r , v_{eff} , and the thickness-dependent variable $\frac{N}{N+1}$ as the third coordinate. In terms of this quantity, the 3D and 2D Ising fixed points assume the values 1 and 0, respectively, and thus become distinguishable. In figures 7–9 we show the trajectories with initial values in the vicinity of the critical temperature for increasing values of the dipole strength. At first the trajectories approach the 3D Ising fixed point, then the 2D Ising fixed point, and finally the asymptotic

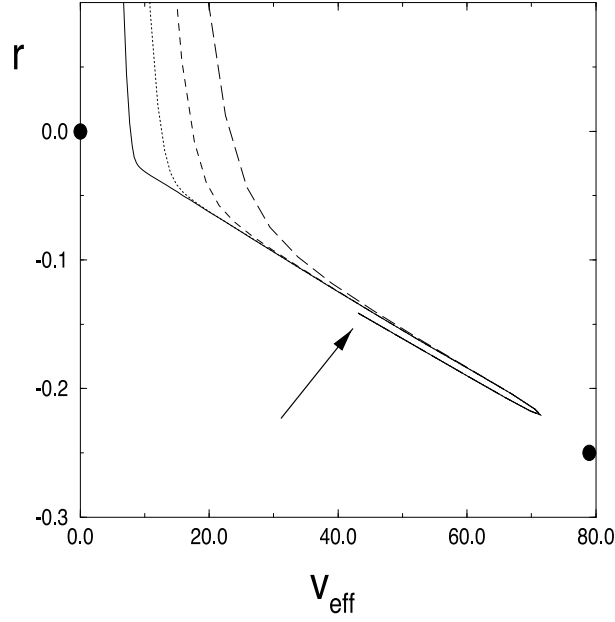


Figure 6. Infinite 3D dipolar system. Flow of the effective coupling v_{eff} and temperature variable r for different initial temperature values, with $g_0 = 10^{-3}$ and $u_0 = 5$: $r \approx r_c$ (full line), $r - r_c = 4.44 \times 10^{-10}$ (dotted), $r - r_c = 4.04 \times 10^{-8}$ (dashed), $r - r_c = 7.40 \times 10^{-7}$ (long-dashed).

2D uniaxial dipolar fixed point. Eventually even the tiny numerical deviation from the critical temperature gives rise to a divergence in r again. For stronger dipole interaction, the Ising fixed points are not approached as closely. In figure 10 we furthermore depict the temperature dependence of the trajectories: the higher the temperature the sooner the trajectories start to diverge.

7. Summary

In this paper we have analysed crossover scenarios for a uniaxial dipolar magnetic layer. We have derived the appropriate effective free energy functional in the long-wavelength limit for a finite system with thickness L in one spatial direction; the resulting dipolar Hamiltonian turned out to be considerably different from the one for the infinite 3D system. In the long-wavelength limit, which does not commute with the limit $L \rightarrow \infty$, the propagator of the 3D system cannot be recovered from the propagator of the layer in the limit of infinite layer thickness.

We have presented a unified renormalization scheme, within which the critical behaviour of the layer with finite thickness can nevertheless be treated as well as that of the infinite system. This renormalization procedure is required to be capable of capturing the crossovers between critical regions with different system dimensions, different analytical structures of the propagator due to the dipole–dipole interaction, and consequently different upper critical dimensions. Hence we had to refrain from any dimensional ϵ expansion near any of the fixed points, and have derived the renormalization group flow equations in the one-loop approximation at fixed dimension. Furthermore, we have introduced a common effective expansion parameter, as suggested by the flow equations, which leads to finite non-trivial fixed points characterizing the different critical regions. As a test of the consistency of our approach,

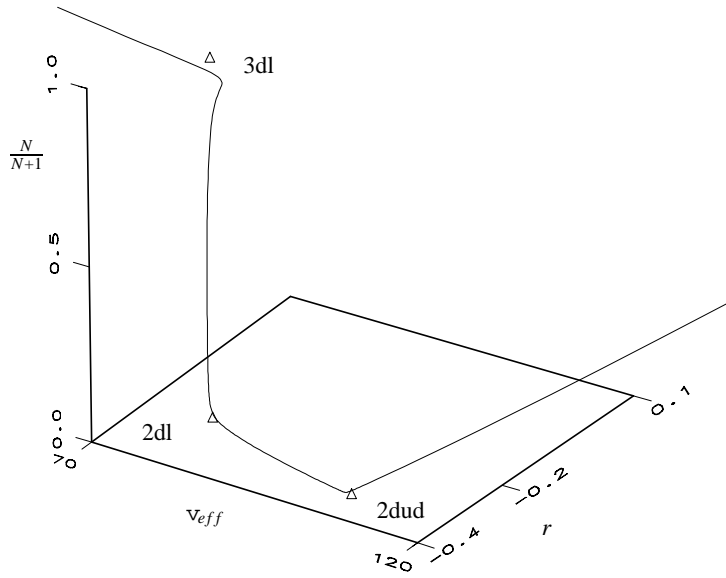


Figure 7. Dipolar layer with easy in-plane axis. Flow diagram for $g_0 = 10^{-7}$, $u_0 = 10$, $r_0 \sim r_c$, $N_0 = 100$.

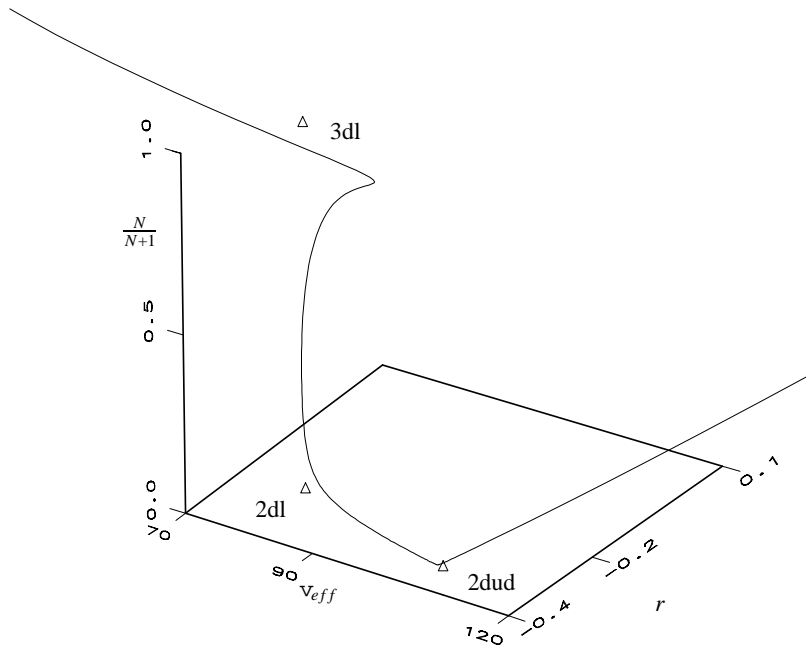


Figure 8. Dipolar layer with easy in-plane axis. Flow diagram for $g_0 = 10^{-6}$, $u_0 = 10$, $r_0 \sim r_c$, $N_0 = 100$.

the critical exponents in the limiting cases of the 3D Ising, 2D Ising, 3D uniaxial dipolar, and 2D uniaxial (in-plane easy axis) dipolar universality classes were calculated within ϵ expansions with respect to the appropriate upper critical dimensions, respectively, and reproduced correctly

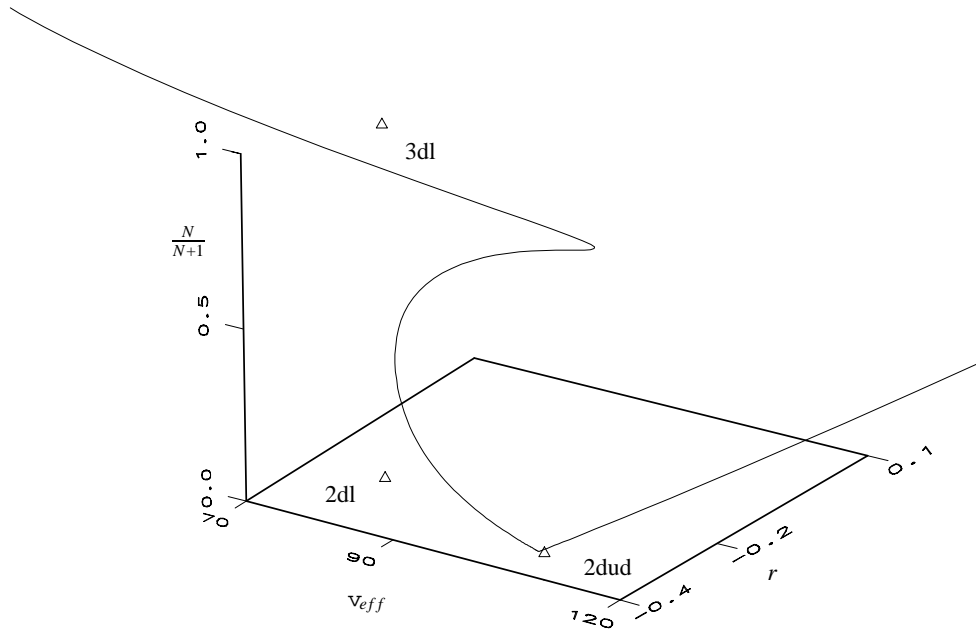


Figure 9. Dipolar layer with easy in-plane axis. Flow diagram for $g_0 = 10^{-5}$, $u_0 = 10$, $r_0 \sim r_c$, $N_0 = 100$.

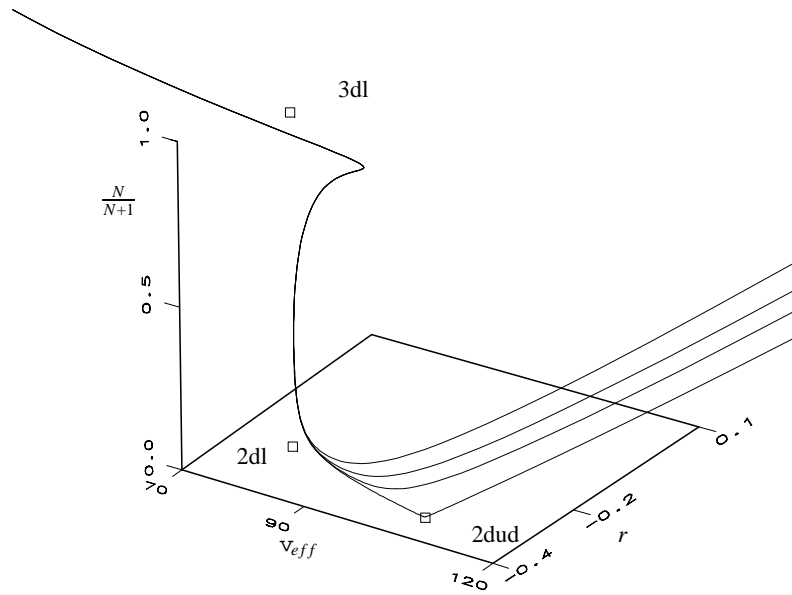


Figure 10. Dipolar layer with easy in-plane axis. Flow diagram for $g_0 = 10^{-6}$, $u_0 = 10$, $r_0 - r_c = 8.33 \times 10^{-10}$, 2.33×10^{-10} , 0.53×10^{-10} , $r_0 \sim r_c$, (from left to right), $N_0 = 100$.

known results from the literature. The critical exponents for the asymptotic limit of a 2D uniaxial dipolar system with in-plane easy axis were, to our knowledge, computed explicitly for the first time by means of an expansion near the upper critical dimension $d_c = \frac{7}{2}$.

Performing the calculations without the ϵ expansion, however, reveals an unfortunate insufficiency of the one-loop approximation: the numerical values of the temperature variable, the effective coupling, and the critical exponents at the 3D and the 2D Ising fixed points happen to be identical in $D = 3$ dimensions. In order to test our scheme, we have first evaluated the dimensional crossover of the effective critical exponent γ_{eff} of an Ising system from $D = 3.2$ to $D = 2.2$ dimensions. Second, the crossover features of the 3D uniaxial dipolar system as well as the uniaxial dipolar layer were analysed and discussed in the form of renormalization group flow diagrams. Thus, we hope to have demonstrated the feasibility of the description of such very complex crossover features within the framework of our renormalization group approach, which should be further applicable to a diverse range of interesting physical systems.

Acknowledgments

We acknowledge support from the German Education and Research Department (BMBF) under contract no 03-SC5-TUM 0, and from the Deutsche Forschungsgemeinschaft (DFG), contract nos Schw 348/12-1 and Ta 177/2-1,2.

Appendix A. Critical temperature

A number of the above calculations depended on the knowledge of the phase transition temperature which, due to thermal fluctuations, is shifted downwards as compared with the mean-field transition temperature. The correct location of the critical point (to one-loop order) was determined numerically through identifying that starting point of the temperature variable r , which separates those renormalization group flow trajectories that eventually flow to $r = +\infty$ from the ones that eventually flow to $r = -\infty$.

Figures A1 and A2 show the dependence of the numerically obtained phase transition temperature r_c upon the strength of the dipole–dipole interaction g and the layer thickness N .

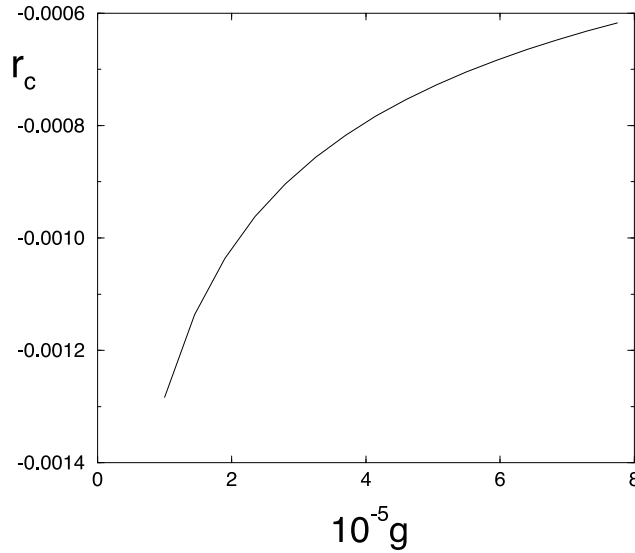


Figure A1. Phase transition temperature $r_c(g)$ versus dipole strength ($N_0 = 100$, $u_0 = 0.1$).

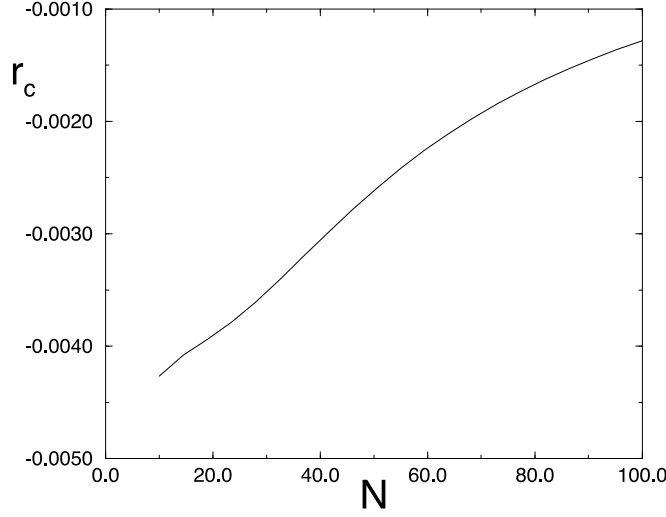


Figure A2. Phase transition temperature $r_c(N)$ versus layer thickness ($g_0 = 1 \times 10^{-5}$, $u_0 = 0.1$).

As one would expect physically, r_c grows both with increasing dipole strength and increasing layer thickness.

Appendix B. Layer with out-of-plane easy axis

As already mentioned, the propagator for the dipolar layer with out-of-plane easy axis,

$$G_0(\mathbf{q}, \mathbf{p})^{-1} = r_0 + c_0 k^2 - g(1 + \tilde{f}_1)p - g\tilde{f}_3 p^2 - g\tilde{f}_2 q^2 p \quad (\text{B.1})$$

is not positive definite under the renormalization group flow. This indicates an instability of the homogeneous ground state at some finite wavevector. Therefore this propagator cannot be used in a straightforward manner for the calculation of the critical behaviour of the system. Nevertheless we can draw some information regarding the instability from it. Thus, from the equation

$$\left. \frac{\partial}{\partial p} \right|_{q=0} (r + ck^2 - g(1 + \tilde{f}_1)p - g\tilde{f}_3 p^2 - g\tilde{f}_2 q^2 p) = 0 \quad (\text{B.2})$$

we may infer the typical size of the structures in the low-temperature phase, as a function of the dipole strength g and the layer thickness L . The result is

$$D_{\text{domain}} = \frac{2\pi [c + g \frac{L}{2} (1 + \frac{L}{2a_0})]}{g(1 + \frac{L}{a_0})} \quad (\text{B.3})$$

i.e., starting from a constant domain size at vanishing layer thickness, the domain size decreases with increasing thickness, runs through a minimum, and finally grows again linearly with L . The result that a layer with an out-of-plane easy axis should condense inhomogeneously is in accordance with [20–22]; but the increase of the domain size is predicted to be proportional to the square root of the layer thickness in [20, 22], and $\sim L^{1/3}$ in [21].

References

- [1] Larkin A L and Khmel'nitskiĭ D E 1969 *Sov. Phys.–JETP* **29** 1123
- [2] Amit D J and Goldschmidt Y Y 1978 *Ann. Phys., NY* **114** 356
- [3] Frey E and Schwabl F 1990 *Phys. Rev. B* **42** 8261
Frey E and Schwabl F 1992 *J. Magn. Magn. Mater.* **104** 204
Frey E 1995 *Physica A* **221** 52
- [4] Frey E, Täuber U C and Schwabl F 1994 *Europhys. Lett.* **26** 413
Frey E, Täuber U C and Schwabl F 1994 *Phys. Rev. E* **49** 5058
- [5] Ried K *et al* 1993 *Phys. Lett. A* **180** 370
Ried K *et al* 1994 *Phys. Rev. B* **49** 4315
Ried K *et al* 1995 *Phys. Rev. B* **51** 15229
- [6] Aharony A 1973 *Phys. Rev. B* **8** 3323
- [7] Rudnick J, Guo H and Jasnow D 1985 *J. Stat. Phys.* **41** 353
- [8] Brezin E and Zinn-Justin J 1985 *Nucl. Phys. B* **257** 867
- [9] Esser A *et al* 1995 *Physica A* **222** 355
Esser A *et al* 1995 *Z. Phys. B* **97** 205
- [10] Chen X S *et al* 1995 *J. Physique* **15** 205
Chen X S *et al* 1996 *Physica A* **232** 375
- [11] Chakravarty S, Halperin B I and Nelson D R 1988 *Phys. Rev. Lett.* **60** 1057
Chakravarty S, Halperin B I and Nelson D R 1989 *Phys. Rev. B* **39** 2344
- [12] O'Connor D and Stephens C R 1991 *Nucl. Phys. B* **360** 297
O'Connor D and Stephens C R 1994 *Phys. Rev. Lett.* **72** 506
- [13] Aharony A 1973 *Phys. Lett. A* **44** 313
- [14] Maleev S V 1976 *Sov. Phys.–JETP* **43** 1240
- [15] Amit D J 1984 *Field Theory, the Renormalization Group, and Critical Phenomena* 2nd edn (Singapore: World Scientific)
- [16] Folk R, Iro H and Schwabl F 1977 *Z. Phys. B* **27** 169
- [17] Fisher M E, Ma S and Nickel B G 1972 *Phys. Rev. Lett.* **29** 917
- [18] De'Bell K and Geldart D J W 1989 *Phys. Rev. B* **39** 743
- [19] Rudnick J and Nelson D R 1976 *Phys. Rev. B* **13** 2208
- [20] Kooy C and Enz U 1960 *Philips Res. Rep.* **15** 7
- [21] Garel T and Doniach S 1982 *Phys. Rev. B* **26** 325
- [22] Kaplan B and Gehring G A 1993 *J. Magn. Magn. Mater.* **128** 111